NACA

RESEARCH MEMORANDUM

A STUDY OF THE USE OF VARIOUS HIGH-LIFT DEVICES ON THE

HORIZONTAL TAIL OF A CANARD AIRPLANE MODEL AS

A MEANS OF INCREASING THE ALLOWABLE

CENTER-OF-GRAVITY TRAVEL

By Joseph L. Johnson, Jr.

Langley Aeronautical Laboratory
Langley Field, Va.

NATIONAL ADVISORY COMMITTEE
FOR AERONAUTICS

WASHINGTON
January 21, 1953

NATIONAL ADVISORY COMMITTEE FOR AERONAUTICS

RESEARCH MEMORANDUM

A STUDY OF THE USE OF VARIOUS HIGH-LIFT DEVICES ON THE

HORIZONTAL TAIL OF A CANARD AIRPLANE MODEL AS

A MEANS OF INCREASING THE ALLOWABLE

CENTER-OF-GRAVITY TRAVEL

By Joseph L. Johnson, Jr.

SUMMARY

An investigation has been made to study the use of various high-lift devices on the horizontal tail of a canard airplane model as a means of increasing the allowable center-of-gravity travel. The results indicated that large increases in allowable center-of-gravity travel could be obtained in this manner. The center-of-gravity travel was not always increased, however, for cases in which the high-lift device increased the tail lift-curve slope and thereby reduced the stability of the configuration. In these cases, the use of high-lift devices linked to deflect automatically in proportion to increases in angle of incidence of the tail appears to offer a means of obtaining the maximum beneficial effect of the high-lift device on the allowable center-of-gravity travel.

INTRODUCTION

Some recent studies made to determine the stability and control characteristics of canard designs have indicated some advantages over conventional configurations at transonic and supersonic speeds. (For example, see ref. 1.) In connection with these general studies two investigations to determine the low-speed static stability and control characteristics of canard designs have been conducted in the Langley free-flight tunnel (refs. 2 and 3). These investigations indicated that the particular canard designs studied had a small allowable center-of-gravity range relative to that of a more conventional-type airplane.

A further study of the longitudinal characteristics of canard designs indicated that the allowable center-of-gravity travel could be

increased if the maximum lift coefficient of the tail were increased to provide additional trimming power. Other studies such as the theoretical work of reference 4 have led to similar conclusions but no experimental data have been available for verification. An investigation was therefore undertaken to study experimentally the use of high-lift devices on the horizontal tail as a means of increasing the trimming power of the tail and thus increasing the allowable center-of-gravity travel of canard designs.

In this investigation force tests were made to determine the longitudinal stability and control characteristics of a canard model having a 45° sweptback wing of aspect ratio 3. The model was tested with a 60° triangular horizontal tail and with a 45° sweptback horizontal tail. Tests were made with trailing-edge split flaps on each horizontal tail. The model was also tested with a leading-edge flap on the sweptback tail and with a leading-edge flap in combination with a trailing-edge split flap on the sweptback tail.

SYMBOLS AND COEFFICIENTS

All forces and moments are measured about the stability axes which are defined in figure 1.

C_L lift coefficient, $\dfrac{\text{Lift}}{qS}$

C_D drag coefficient, $\dfrac{\text{Drag}}{qS}$

C_N normal-force coefficient, $\dfrac{\text{Normal force}}{qS}$

C_m pitching-moment coefficient, $\dfrac{\text{Pitching moment}}{qS\bar{c}}$

q dynamic pressure, $\frac{1}{2}\rho V^2$, lb/sq ft

ρ air density, slugs/cu ft

V airspeed, ft/sec

S wing area, sq ft

b wing span, ft

$\bar{c}$ mean aerodynamic chord of wing, ft

α angle of attack of fuselage center line, deg

i_t incidence of horizontal tail, positive with leading edge up, deg

l tail length, ft

h distance from center of gravity to neutral point, ft

x distance from aerodynamic center of wing-fuselage combination to neutral point, ft

$\dfrac{\partial C_m}{\partial C_L}$ static margin, $-\dfrac{h}{\bar{c}}$, chords

$C_{L_\alpha} = \dfrac{\partial C_L}{\partial \alpha}$ per deg

$C_{D_\alpha} = \dfrac{\partial C_D}{\partial \alpha}$ per deg

$C_{N_\alpha} = \dfrac{\partial C_N}{\partial \alpha}$ per deg

Subscripts:

t horizontal tail (tail coefficients based on tail area)

wf wing-fuselage combination

APPARATUS AND TESTS

The investigation was conducted in the Langley free-flight tunnel. A three-view drawing of the model used in the investigation is shown in figure 2, and the physical characteristics of the model are presented in table I. The model had a fuselage of circular cross section and a 45° sweptback wing of NACA 0012 airfoil section. Two horizontal tails having the same areas (0.15 wing area) but different plan forms were used in the investigation. One horizontal tail had a 60° triangular plan form and flat-plate airfoil section; the other had the same plan form and airfoil section as the wing. The trailing-edge split flaps and leading-edge flap used on the model are shown in figure 2.

Force tests were made to determine the aerodynamic characteristics of the model with the triangular horizontal tail, with the sweptback

horizontal tail, and with the horizontal tail removed. The longitudinal characteristics were determined with trailing-edge split flaps on each horizontal tail. The model was also tested with a leading-edge flap on the sweptback tail and with a leading-edge flap in combination with a trailing-edge flap on the sweptback tail. Tests were made at zero side-slip over an angle-of-attack range for angles of tail incidences ranging from $0°$ to $20°$.

All the force tests were made at a dynamic pressure of 3.0 pounds per square foot, which corresponds to an airspeed of about 34.0 miles per hour at standard sea-level conditions and to a Reynolds number of approximately 443,000 based on the wing mean aerodynamic chord of 1.38 feet. All moment data are referred to a center-of-gravity position of 24.0 percent of the mean aerodynamic chord ahead of the leading edge of the mean aerodynamic chord unless otherwise noted.

ANALYSIS

The allowable center-of-gravity travel can be defined as the distance, in terms of the mean aerodynamic chord of the wing, between the forward and rearward limits of the center-of-gravity position. In the present investigation the forward limit is designated as the most forward center-of-gravity position at which the model can be trimmed to the maximum tail-off lift coefficient (approximately 0.9 for this investigation). The rearward limit is designated as the most rearward center-of-gravity position at which the model is at least neutrally stable $\left(\dfrac{\partial C_m}{\partial C_L} = 0\right)$.

The following equation for computing the allowable center-of-gravity travel is developed in the appendix:

$$\frac{h}{\bar{c}} = \frac{\dfrac{l}{\bar{c}}\left(1 - \dfrac{C_{N_{\alpha_t}}}{C_{N_{\alpha_{wf}}}}\dfrac{C_{N_{wf}}}{C_{N_t}}\right)}{\dfrac{C_{N_{wf}}}{C_{N_t}}\dfrac{S_t}{S} + \dfrac{C_{N_{\alpha_t}}}{C_{N_{\alpha_{wf}}}}\dfrac{C_{N_{wf}}}{C_{N_t}}} \qquad (1)$$

Equation (1) was derived by neglecting downwash and interference effects between the tail and wing-fuselage combination and by assuming linear variations of all the factors involved. The use of isolated tail and wing data in equation (1) requires correction for downwash and

interference effects if reasonable accuracy is expected in the pre-
dicted values of the allowable center-of-gravity travel.

An examination of equation (1) shows that the allowable center-of-
gravity travel increases with an increase in the maximum normal-force
coefficient of the tail or a. decrease in the slope of the normal-force-
coefficient curve of the tail. Any increase in the maximum normal-
force coefficient of the wing or decrease in slope of the normal-force-
coefficient curve of the wing would, of course, decrease the allowable
center-of-gravity travel if trim at a higher lift coefficient is desired.

If the use of a high-lift device on the tail increases the slope
of the normal-force-coefficient curve of the tail as well as the maximum
normal-force coefficient, then the allowable center-of-gravity travel
may be increased or decreased or may remain unchanged depending upon the
magnitude of $C_{N_{t_{max}}}$ and $C_{N_{\alpha t}}$. In such cases, the use of high-lift
devices on the horizontal tail which are linked to deflect automatically
in proportion to increases in angle of incidence of the tail (angle of
horizontal tail with respect to longitudinal axis of fuselage) appears
to offer a means of increasing the allowable center-of-gravity travel.
In this manner, a forward shift in the forward limit of the center of
gravity is obtained while the rearward limit remains in the same posi-
tion as that of the basic configuration.

RESULTS AND DISCUSSION

Basic Aerodynamic Data

The aerodynamic characteristics of the model with the horizontal
tail off and with either the triangular tail or the sweptback tail on
are presented in figure 3. These data show that the wing-fuselage com-
bination had a maximum lift coefficient of approximately 0.95. The
model had a slightly higher maximum lift coefficient and greater static
longitudinal stability $-\partial C_M/\partial C_L$ with the triangular tail than with the
sweptback tail. Both configurations had a maximum trim lift coefficient
of about 0.7 with the center of gravity located 0.24 mean aerodynamic
chord ahead of the leading edge of the mean aerodynamic chord and showed
similar trends in the pitching-moment characteristics. That is, at low
lift coefficients an increase in incidence of the tail gave a positive
increment to the pitching-moment coefficient with little change in sta-
bility. In the higher lift-coefficient range, however, an increase in
angle of incidence caused the horizontal tail to stall, which resulted
in a loss of control effectiveness and in an increase in stability of
the model.

The aerodynamic characteristics of the model with split flaps added to the triangular tail and to the sweptback tail are presented in figure 4. These data show an increase in maximum trim lift coefficient of both configurations to 0.9 and little change in stability or maximum lift coefficient over the basic configuration.

The aerodynamic characteristics of the model with the sweptback tail having a leading-edge flap and a leading-edge flap in combination with a trailing-edge flap are presented in figure 5. The addition of the leading-edge flap to the tail produced about the same maximum trim lift coefficient of the model as the split-flap arrangement but reduced the stability of the model. The combination flaps increased the maximum trim lift coefficient to 1.1 but produced a greater decrease in stability than the leading-edge flap.

Effect of Tail Configuration on the Allowable

Center-of-Gravity Travel

In order to determine the allowable center-of-gravity travel for each of the configurations tested, the aerodynamic data of figures 3, 4, and 5 were transferred to the most forward center-of-gravity position at which the model could be trimmed to lift coefficient of 0.9. These data, presented in figure 6, include the pitching-moment curve for $0°$ incidence and also the curve for the angle of incidence for which maximum trim lift coefficient was obtained for each configuration. Included with the data for the flap-on configurations is the pitching-moment curve for $0°$ incidence for the flap-off configuration so that the effect of flap deflection on the stability of the model can be seen directly from figure 6. The allowable center-of-gravity travel can be determined from figure 6 by measuring the slope of the pitching-moment curves for $0°$ incidence since this slope represents the distance in mean aerodynamic chords between the most forward center-of-gravity position and the neutral point (most rearward center-of-gravity position).

In the following discussion, the effect of flaps on the allowable center-of-gravity travel is considered with the flaps fully deflected for all angles of incidence of the horizontal tail and, also, with the flaps linked to deflect automatically in proportion to increases in angle of incidence of the tail. For the linked-flap-deflection case, the forward center-of-gravity position is obtained from the flap-extended data, while the rearward position is obtained from the flap-retracted data. No experimental data were obtained for the intermediate flap deflections which would be required with the intermediate tail incidence for a linked flap arrangement. It is assumed, however, that the intermediate flap settings and tail incidences would provide a gradual change between the pitching characteristics for the flap-retracted

and flap-extended cases presented in figure 6. As previously mentioned, when the addition of a flap has no effect on the slope of the normal-force-coefficient curve of the tail there is no advantage in having the linked flap.

In order to provide information which would be helpful in interpreting the data of figure 6, the normal-force coefficients for each tail configuration were determined from the incremental pitching-moment data of figures 3 to 5 and are presented in figure 7. A summary plot showing the allowable center-of-gravity travel as well as the most forward and most rearward center-of-gravity positions is presented in figure 8.

Flaps retracted.- The data of figure 8 show that the model with triangular tail had $0.10\bar{c}$ allowable center-of-gravity travel, whereas the model with the sweptback tail had only $0.04\bar{c}$ allowable center-of-gravity travel. This difference can be attributed to the fact that the triangular tail has both a lower slope of the normal-force-coefficient curve and a higher maximum normal-force coefficient. The increase in maximum normal-force coefficient of the triangular tail gave a more forward limit of the allowable center-of-gravity travel and the decrease in slope of the normal-force-coefficient curve of the triangular tail gave a more rearward limit of the allowable center-of-gravity travel.

Trailing-edge split flaps extended.- The addition of trailing-edge split flaps to the horizontal tail increased the allowable center-of-gravity travel to $0.18\bar{c}$ for the triangular-tail configuration and to $0.14\bar{c}$ for the sweptback-tail configuration. Since the addition of the split flaps increased the maximum normal-force coefficient without changing the slope of the normal-force-coefficient curve of the tails (fig. 7), the allowable center-of-gravity travel was increased because the forward limit was shifted to a more forward station, whereas the rearward limit remained the same as that of the basic configuration. The use of linked flaps in these cases provided little or no improvement in the allowable center-of-gravity travel.

Leading-edge flap extended.- The addition of a leading-edge flap to the sweptback tail increased the allowable center-of-gravity travel of the model to $0.05\bar{c}$. The data of figure 8 show that the rearward limit as well as the forward limit of the allowable center-of-gravity travel was shifted to a more forward station on the model. This forward shift in the allowable center-of-gravity range results from the fact that the leading-edge flap increased the slope of the normal-force-coefficient curve as well as the maximum normal-force coefficient (fig. 7). The use of a linked leading-edge flap would result in an increase in the allowable center-of-gravity travel to $0.16\bar{c}$.

In the present investigation, a relatively large leading-edge flap was used in an effort to obtain a high maximum normal-force coefficient of the tail. This flap, however, resulted in an increase in the slope of the normal-force-coefficient curve as well as the maximum normal-force coefficient. The use of a leading-edge flap which would provide no increase in slope of the tail normal-force-coefficient curve would probably give a greater allowable center-of-gravity travel than the flap used even though it might provide a lower maximum tail normal-force coefficient.

Leading-edge and trailing-edge split flaps extended.- The use of a leading-edge flap and a trailing-edge split flap in combination on the sweptback tail increased the allowable center-of-gravity travel to $0.10\bar{c}$. The data of figure 7 show that these flaps gave the largest value of the maximum normal-force coefficient of the tail and, as in the case of the leading-edge flap alone, increased the slope of the normal-force-coefficient curve of the tail. As a result of the high maximum normal-force coefficient, the forward limit of the allowable center-of-gravity travel was shifted to a more forward station on the model than was obtained with any of the other configurations. The rearward limit was also shifted forward so that the over-all increase in the allowable center-of-gravity travel was not very great. The use of linked flaps would result in an increase in the allowable center-of-gravity travel of $0.24\bar{c}$.

It appears that the use of high-lift devices more powerful than those of the present investigation offers greater possibilities for increasing the allowable center-of-gravity travel of a canard design. High-lift devices such as the double-slotted flap or the Fowler flap or combinations of these trailing-edge flaps with leading-edge flaps should increase the maximum normal-force coefficient of the tail to 2.0 or even higher, in which case the allowable center-of-gravity travel of the canard design would probably be increased to values much higher than those shown in the present report.

Comparison of Measured and Predicted Values of the

Allowable Center-Of-Gravity Travel

The allowable center-of-gravity travel for the configurations of the model investigated were calculated from equation (1). For these calculations, the normal-force-coefficient curves for the sweptback horizontal tail, with and without the leading-edge flap, were obtained from unpublished force tests in the Langley free-flight tunnel. The increment of normal-force coefficient resulting from deflecting a trailing-edge split flap on this tail was estimated from the higher-scale tests of reference 5. The normal-force-coefficient curve for the

triangular tail was obtained from tests in the Langley free-flight tunnel of a plan form geometrically similar to that of the tail used on the model (ref. 6). The increment of normal-force coefficient resulting from deflecting a trailing-edge split flap on this tail was estimated from the higher-scale tests of reference 7.

The results of these calculations and the parameters used in making the calculations are presented along with the measured results in figure 9 and table II. The results of figure 9 indicate that the maximum normal-force coefficients measured from the model force tests of this report are generally smaller than those obtained from tests of isolated surfaces. The measured and predicted slopes of the normal-force-coefficient curves are in good agreement except for the leading-edge flap configurations, which have higher measured values than estimated values. The difference between the measured and predicted maximum normal-force coefficients and slopes of the normal-force-coefficient curves is attributed to downwash and to interference effects between the tail and wing-fuselage combination. For instance, the gap between the horizontal tail and fuselage could be a factor which greatly alters the predicted characteristics of the tail. Because of these differences, the values of the allowable center-of-gravity travel as determined from equation (1) are much larger than those measured from the model data of this report. It appears from these results that accurate estimation of the center-of-gravity travel is impossible at the present time because of the difficulties involved in accounting for the downwash and interference effects. Further work is necessary, therefore, to determine these effects before use of isolated-tail data can be made to predict the allowable center-of-gravity travel.

CONCLUDING REMARKS

The following conclusions were drawn from the results of the investigation to study the use of various high-lift devices on the horizontal tail of a canard airplane model as a means of increasing the allowable center-of-gravity travel.

1. The addition of high-lift devices to the horizontal tail considerably increased the allowable center-of-gravity travel because of increased trimming power of the tail.

2. The center-of-gravity travel was not always increased, however, for cases in which the high-lift device increased the tail lift-curve slope and thereby reduced the stability of the configuration.

3. When the stability of a model was reduced by the addition of high-lift devices to the horizontal tail, the use of high-lift devices

linked to deflect automatically in proportion to an increase in angle of incidence of the tail appeared to offer a means of obtaining the maximum beneficial effect of these high-lift devices on the allowable center-of-gravity travel.

Langley Aeronautical Laboratory,
National Advisory Committee for Aeronautics,
Langley Field, Va.

APPENDIX

DERIVATION OF AN EXPRESSION FOR DETERMINING THE ALLOWABLE

CENTER-OF-GRAVITY TRAVEL OF A CANARD DESIGN

A qualitative estimation of the longitudinal stability of a canard design can be made analytically by considering the relation between the lift and drag forces of the tail and those of the wing-fuselage combination as illustrated in the following sketch:
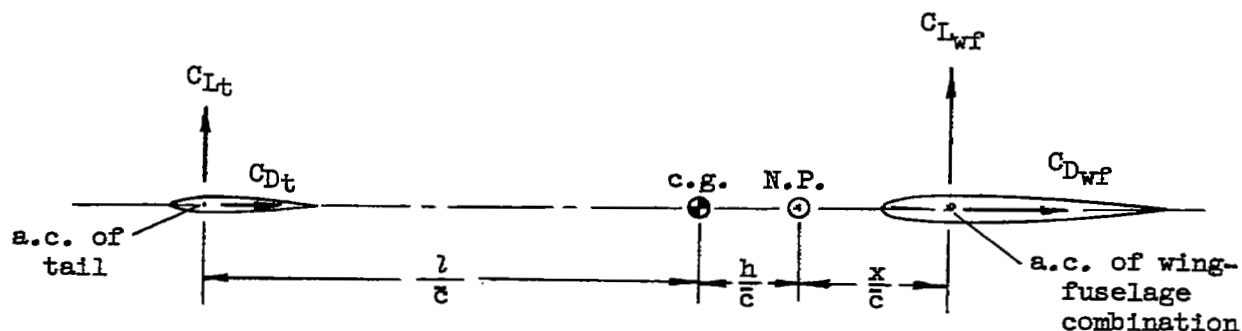
Assuming that the center of gravity is in the horizontal plane of the aerodynamic centers of the wing and tail, an expression for the longitudinal stability of the configuration can be written as follows:

$$\frac{\partial C_{L_t}}{\partial \alpha} \frac{l+h}{\bar{c}} \frac{S_t}{S} \cos \alpha + \frac{\partial C_{D_t}}{\partial \alpha} \frac{l+h}{\bar{c}} \frac{S_t}{S} \sin \alpha = \frac{\partial C_{L_{wf}}}{\partial \alpha} \frac{x}{\bar{c}} \cos \alpha + \frac{\partial C_{D_{wf}}}{\partial \alpha} \frac{x}{\bar{c}} \sin \alpha$$

or

$$\frac{\partial C_{N_t}}{\partial \alpha} \frac{l+h}{\bar{c}} \frac{S_t}{S} = \frac{\partial C_{N_{wf}}}{\partial \alpha} \frac{x}{\bar{c}} \tag{A1}$$

An equation can also be written for the relation of the normal-force coefficients of the wing and tail for trim

$$C_{N_t} \frac{l}{\bar{c}} \frac{S_t}{S} = C_{N_{wf}} \frac{h+x}{\bar{c}} \tag{A2}$$

Solving equations (A1) and (A2) simultaneously to eliminate $\frac{x}{c}$ gives the following expression for the allowable center-of-gravity travel:

$$\frac{h}{c} = \frac{\dfrac{l}{c}\left(1 - \dfrac{C_{N_{\alpha_t}}}{C_{N_{\alpha_{wf}}}}\dfrac{C_{N_{wf}}}{C_{N_t}}\right)}{\dfrac{C_{N_{wf}}}{C_{N_t}\dfrac{S_t}{S}} + \left(\dfrac{C_{N_{\alpha_t}}}{C_{N_{\alpha_{wf}}}}\dfrac{C_{N_{wf}}}{C_{N_t}}\right)} \tag{A3}$$

REFERENCES

1. Mathews, Charles W.: A Study of the Canard Configuration With Particular Reference to Transonic Flight Characteristics and Low-Speed Characteristics at High Lift. NACA RM L8G14, 1949.

2. Bates, William R.: Low-Speed Static Longitudinal Stability Characteristics of a Canard Model Having a 60° Triangular Wing and Horizontal Tail. NACA RM L9H17, 1949.

3. Draper, John W.: Low-Speed Static Stability Characteristics of a Canard Model With a 45° Sweptback Wing and a 60° Triangular Horizontal Control Surface. NACA RM L50G11, 1950.

4. Gates, S. B.: Notes on the Tail-First Aeroplane. R. & M. No. 2676, British A. R. C., 1939.

5. Queijo, M. J., and Lichtenstein, Jacob H.: The Effects of High-Lift Devices on the Low-Speed Stability Characteristics of a Tapered 37.5° Sweptback Wing of Aspect Ratio 3 in Straight and Rolling Flow. NACA RM L8I03, 1948.

6. McKinney, Marion O., Jr., and Drake, Hubert M.: Flight Characteristics at Low Speed of Delta-Wing Models. NACA RM L7K07, 1948.

7. Anderson, Adrien E.: An Investigation at Low Speed of a Large-Scale Triangular Wing of Aspect Ratio Two.- I. Characteristics of a Wing Having a Double-Wedge Airfoil Section With Maximum Thickness at 20-Percent Chord. NACA RM A7F06, 1947.

TABLE I.- DIMENSIONAL CHARACTERISTICS OF CANARD MODEL TESTED

IN THE LANGLEY FREE-FLIGHT TUNNEL

Wing:
   Airfoil section . . . . NACA 0012
   Area, sq ft 5.33
   Span, ft 4.00
   Aspect ratio 3.00
   Incidence, deg 0
   Dihedral, deg 0
   Taper ratio 0.5
   Mean aerodynamic chord, ft 1.383
   Root chord, ft 1.77
   Sweepback, leading edge, deg 45

Tip vertical tails:
   Area, sq ft (2 tails) 0.533
   Span, ft 0.63
   Root chord, ft 0.562
   Taper ratio 0.50
   Aspect ratio 1.49

Center vertical tail:
   Area, sq ft 0.272
   Span, ft 0.73
   Root chord, ft 0.495
   Taper ratio 0.50
   Aspect ratio 1.96

Horizontal tail (triangular):
   Airfoil section . . . . Flat plate
   Area, sq ft 0.800
   Span, ft 1.36
   Sweepback, leading edge, deg 60
   Aspect ratio 2.31
   Split flap, deflected, deg 30
     Chord, percent of root chord of tail 15

TABLE I.- DIMENSIONAL CHARACTERISTICS OF CANARD MODEL TESTED

IN THE LANGLEY FREE-FLIGHT TUNNEL - Concluded

Horizontal tail (sweptback):
  Airfoil section . . . . NACA 0012
  Area, sq ft 0.800
  Span, ft 1.54
  Sweepback, leading edge, deg 45
  Aspect ratio 2.97
  Split flap, deflected, deg 60
    Chord, percent of chord of tail 20
  Leading-edge flap, deflected, deg 65
    Chord, percent of chord of tail 17
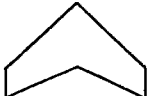
TABLE II.- MEASURED AND PREDICTED VALUES OF THE ALLOWABLE CENTER-OF-GRAVITY
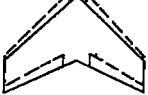
TRAVEL FOR THE MODEL CONFIGURATIONS INVESTIGATED

$$\left[C_{N_{\alpha_{wf}}} = 0.055 \text{ (taken from fig. 3)}; \; C_{N_{wf}} \text{ taken from figure 3}; \right.$$
$$l/\bar{c} = 2.18; \; S_t/S = 0.15; \; C_{L_{t_{max}}} + C_{L_{wf}} = 0.9;$$
$$\left. C_{N_{t_{max}}} + C_{N_{wf}} = C_{N_{model}} \text{ at } C_L = 0.9 \right]$$

Configuration	Measured			Predicted		
	$C_{N_{t_{max}}}$ (a)	$C_{N_{\alpha_t}}$ (a)	h/c̄ (b)	$C_{N_{t_{max}}}$ (c)	$C_{N_{\alpha_t}}$ (c)	h/c̄ (d)
Triangular tail	0.85	0.040	10	1.39	0.043	31
Triangular tail + split flap	1.05	.040	18	1.43	.043	32
Triangular tail + linked split flap	1.05	.040	18	1.43	.043	32
Sweptback tail	0.84	.045	4	0.87	.045	7
Sweptback tail + split flap	1.08	.045	14	1.36	.045	29

Configuration	Measured			Predicted		
	$C_{N_{t_{max}}}$ (a)	$C_{N_{\alpha_t}}$ (a)	h/c̄ (b)	$C_{N_{t_{max}}}$ (c)	$C_{N_{\alpha_t}}$ (c)	h/c̄ (d)
Sweptback tail + linked split flap	1.08	.045	16	1.36	.045	29
Sweptback tail + leading-edge flap	1.00	.060	5	1.36	.054	24
Sweptback tail + linked leading-edge flap	1.00	.045	16	1.36	.045	29
Sweptback tail + leading-edge and split flaps	1.27	.070	10	1.80	.054	49
Sweptback tail + linked leading-edge and split flaps	1.27	.045	24	1.80	.045	55

[a]Measured from figure 7
[b]Measured from figure 6
[c]Taken from unpublished data and references 5, 6, and 7.
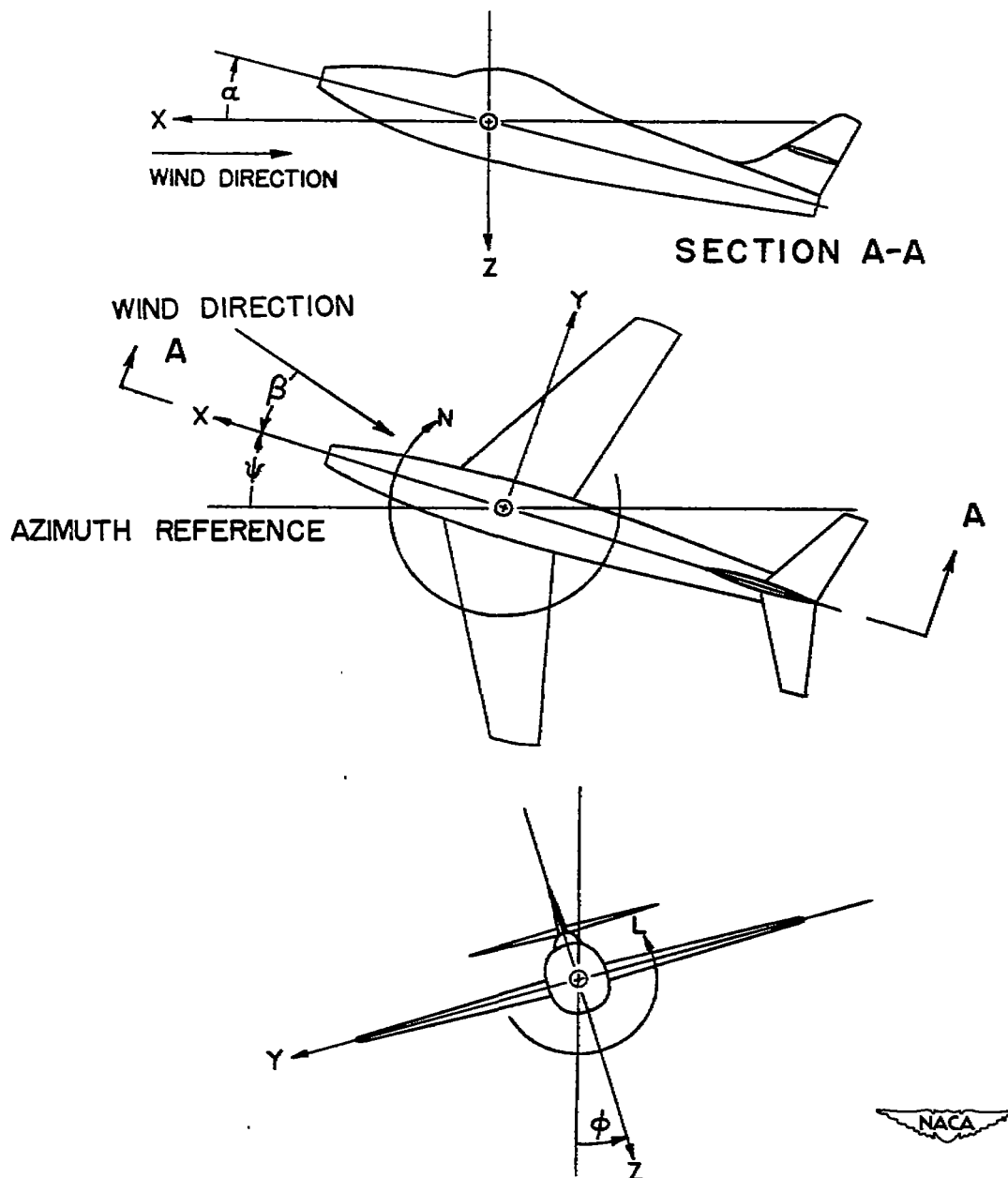[d]Calculated from equation (1)

Figure 1.- The stability system of axes. Arrows indicate positive directions of moments, forces, and angles. This system of axes is defined as an orthogonal system having the origin at the center of gravity and in which the Z-axis is in the plane of symmetry and perpendicular to the relative wind, the X-axis is in the plane of symmetry and perpendicular to the Z-axis, and the Y-axis is perpendicular to the plane of symmetry. At a constant angle of attack, these axes are fixed in the airplane.

30°

15% root chord

Cross section of trailing-
edge split flap parallel
to root chord of tail.

Trailing-edge
split flap

60°

Triangular horizontal tail

16.60

MAC

10.67

45°   6.67

34.28

Trailing-edge
split flap

45°

Leading-edge flap

17% chord

65°   .125

Cross section of leading-
edge flap normal to
leading edge of horizontal
tail.

60°

20% chord

Cross section of trailing-
edge split flap parallel
to root chord of tail.

48.00

5.98

NACA

40.95

70.00
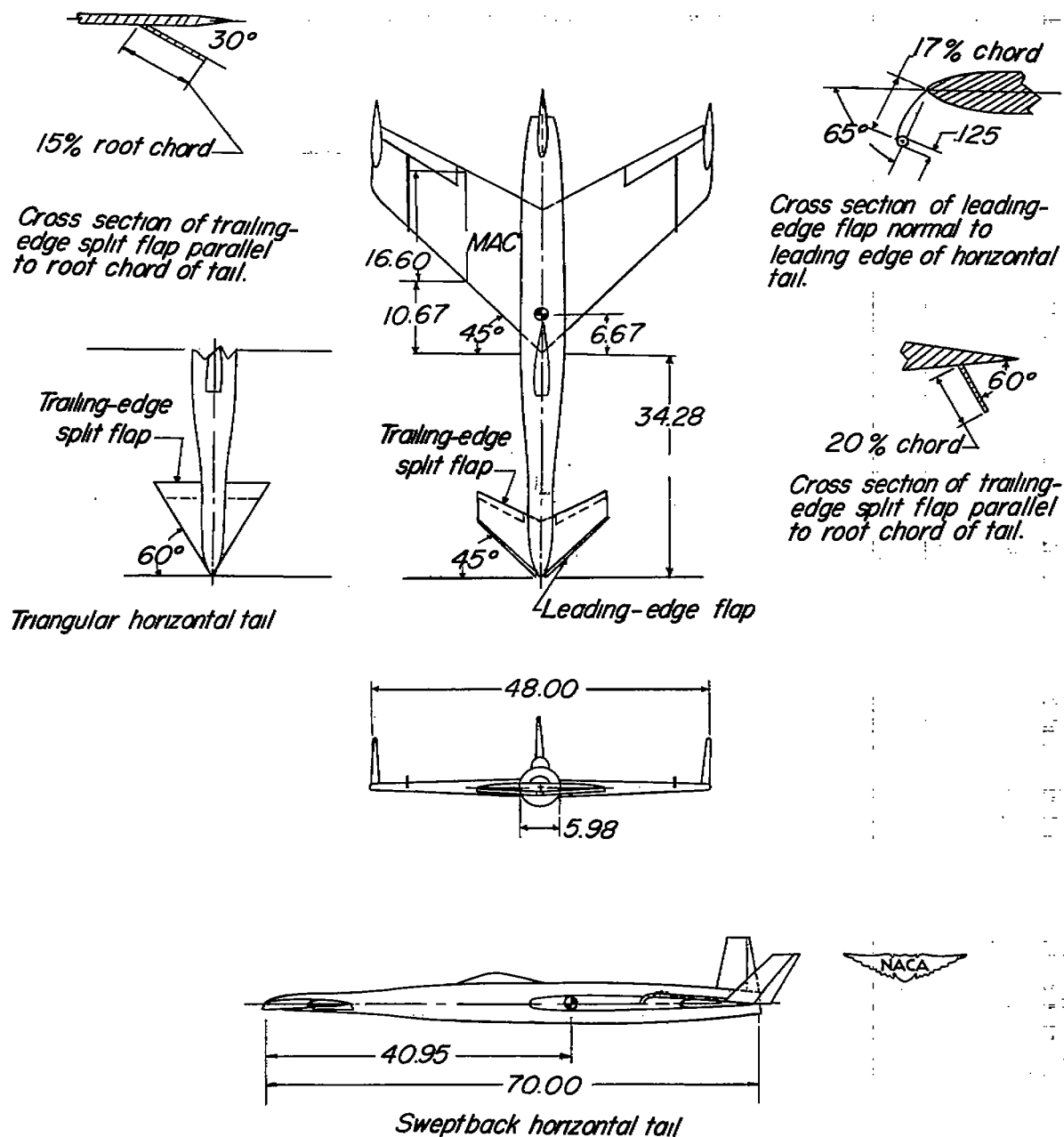
Sweptback horizontal tail

Figure 2.- Three-view drawing of canard model used in the investigation
in the Langley free-flight tunnel. All dimensions are in inches.

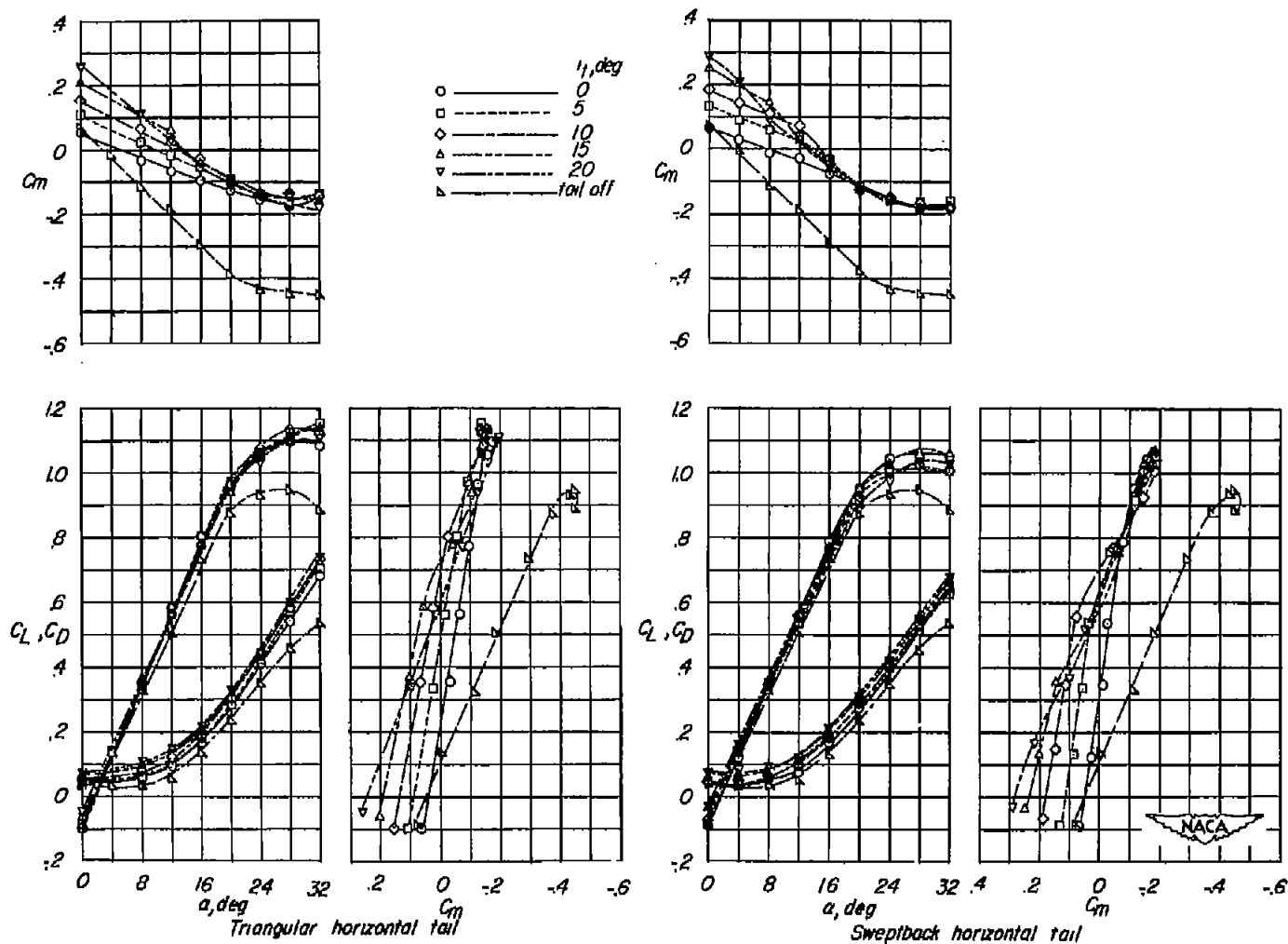Figure 3.- Aerodynamic characteristics of the canard model used in the
investigation. Flaps retracted. Center of gravity, $0.24\bar{c}$ ahead of
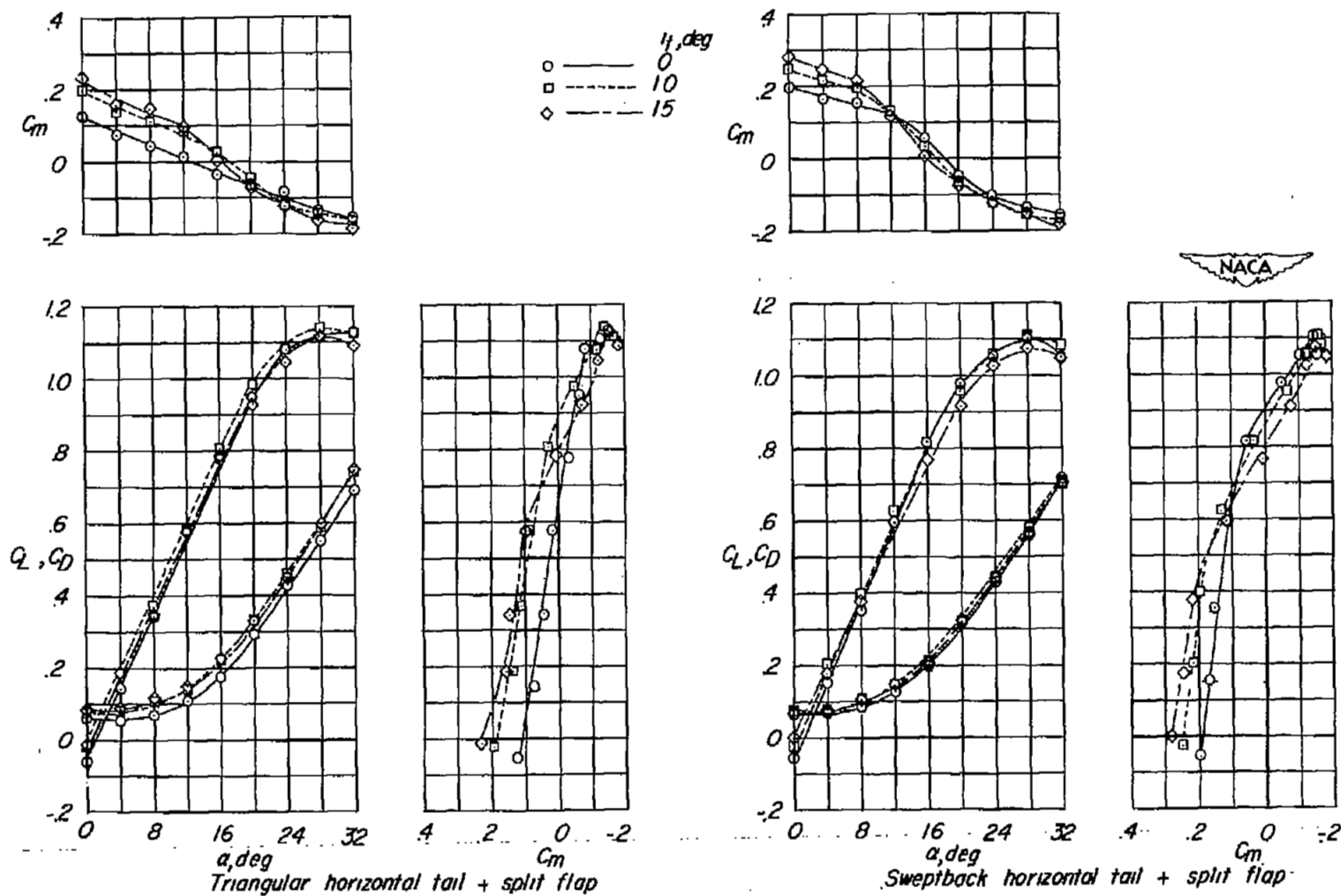leading edge of $\bar{c}$.

Figure 4.- Aerodynamic characteristics of the canard model used in the
investigation. Trailing-edge split flaps extended. Center of
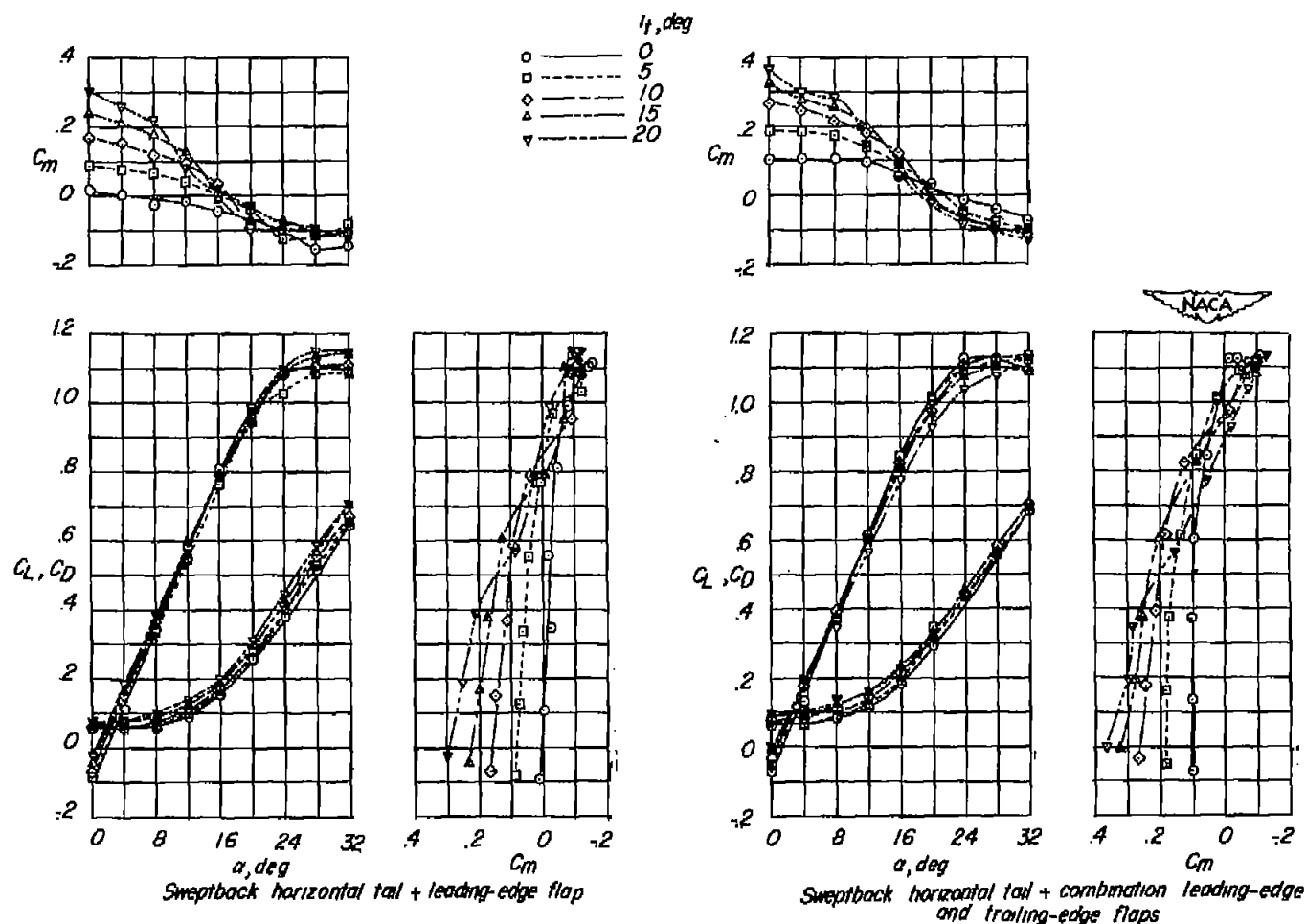gravity, 0.24c̄ ahead of leading edge of c̄.

Figure 5.- Aerodynamic characteristics of the canard model used in the investigation. Leading-edge flap or combination of leading-edge and trailing-edge flaps extended. Center of gravity, $0.24\bar{c}$ ahead of leading edge of $\bar{c}$.
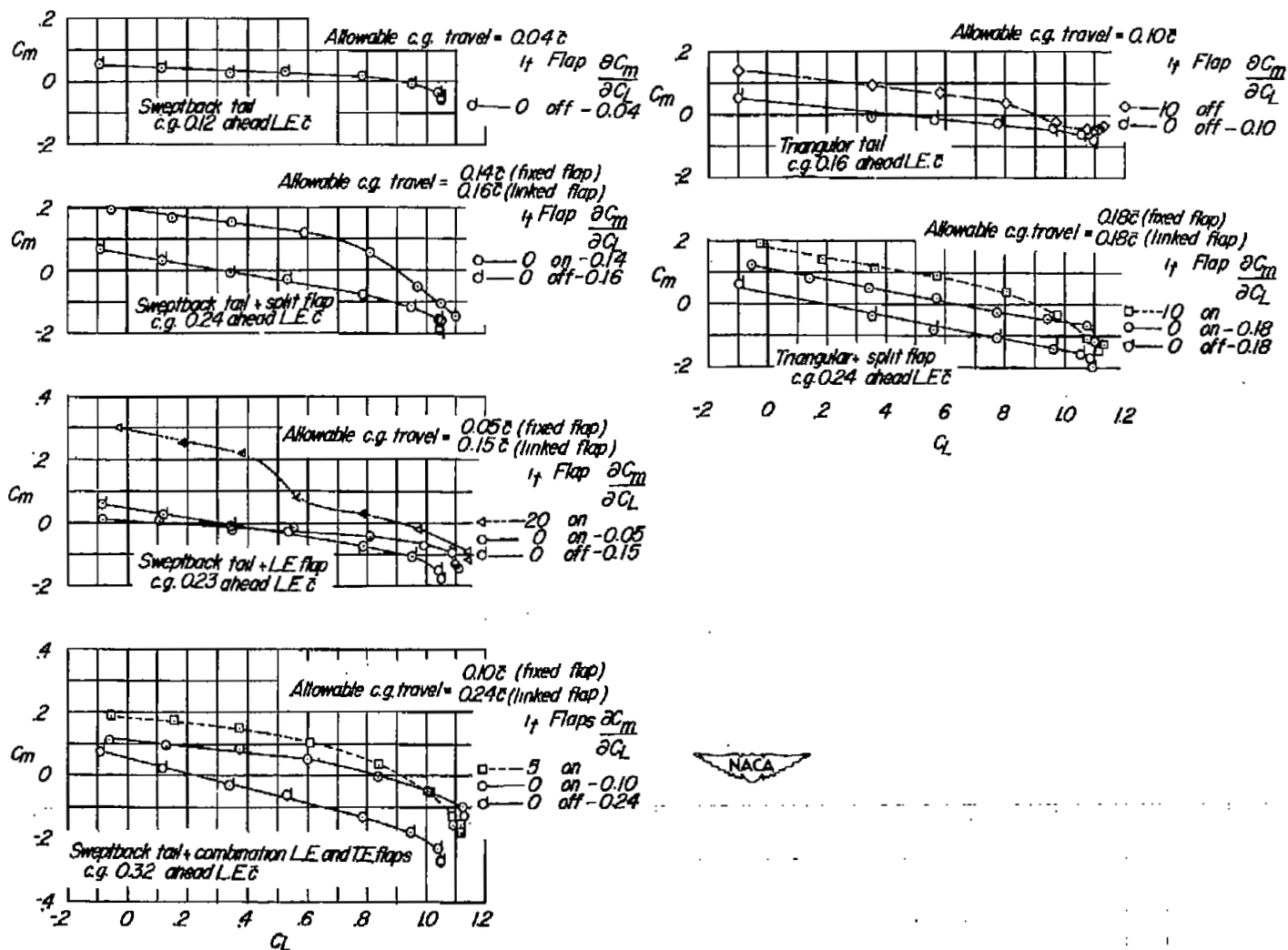
Figure 6.- Longitudinal stability characteristics of the canard model
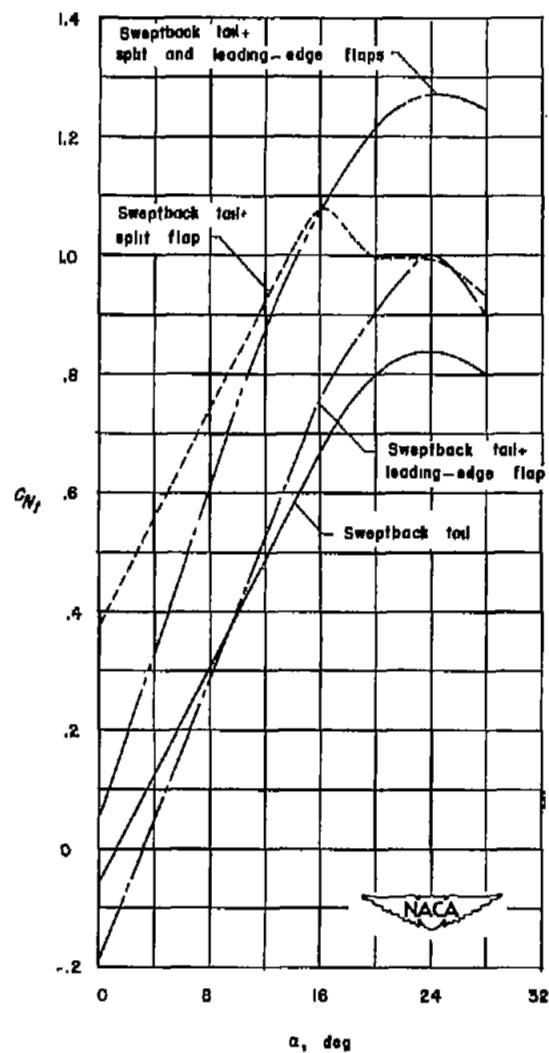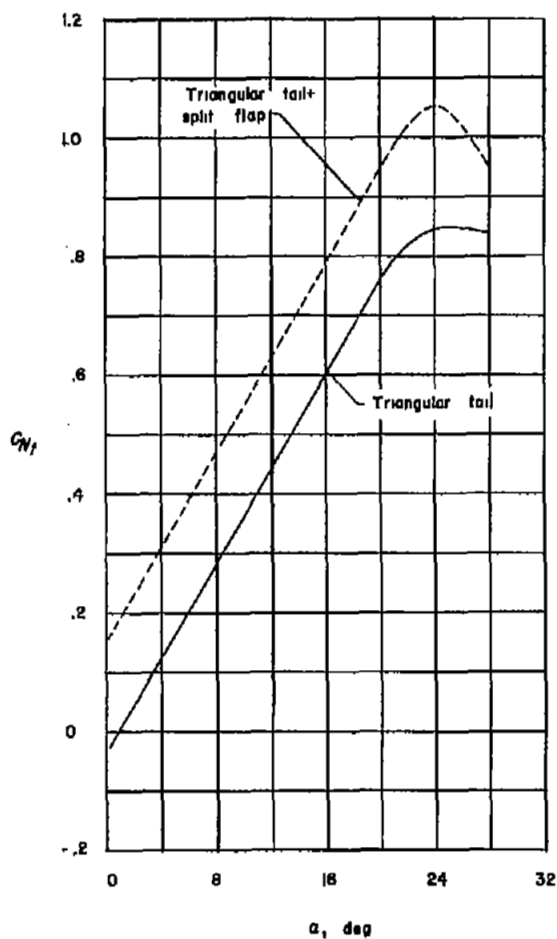used in the investigation.

Figure 7.- Normal-force coefficients of the triangular and sweptback horizontal tail.

CONFIDENTIAL

Model configuration

Allowable c.g.travel,
percent c̄

Most forward   Most rearward

triangular tail   10

triangular tail+ split flap   18

triangular tail+   linked   split flap   18

sweptback tail   4

sweptback tail+split flap   14

sweptback tail+   linked split flap   16

sweptback tail+ L.E. flap   5

sweptback tail+   linked L.E.flap   15

sweptback tail+ combination
L.E.and T.E. flaps   10

sweptback tail+ linked
combination L.E.and T.E. flaps   24

32   24   16   8   0
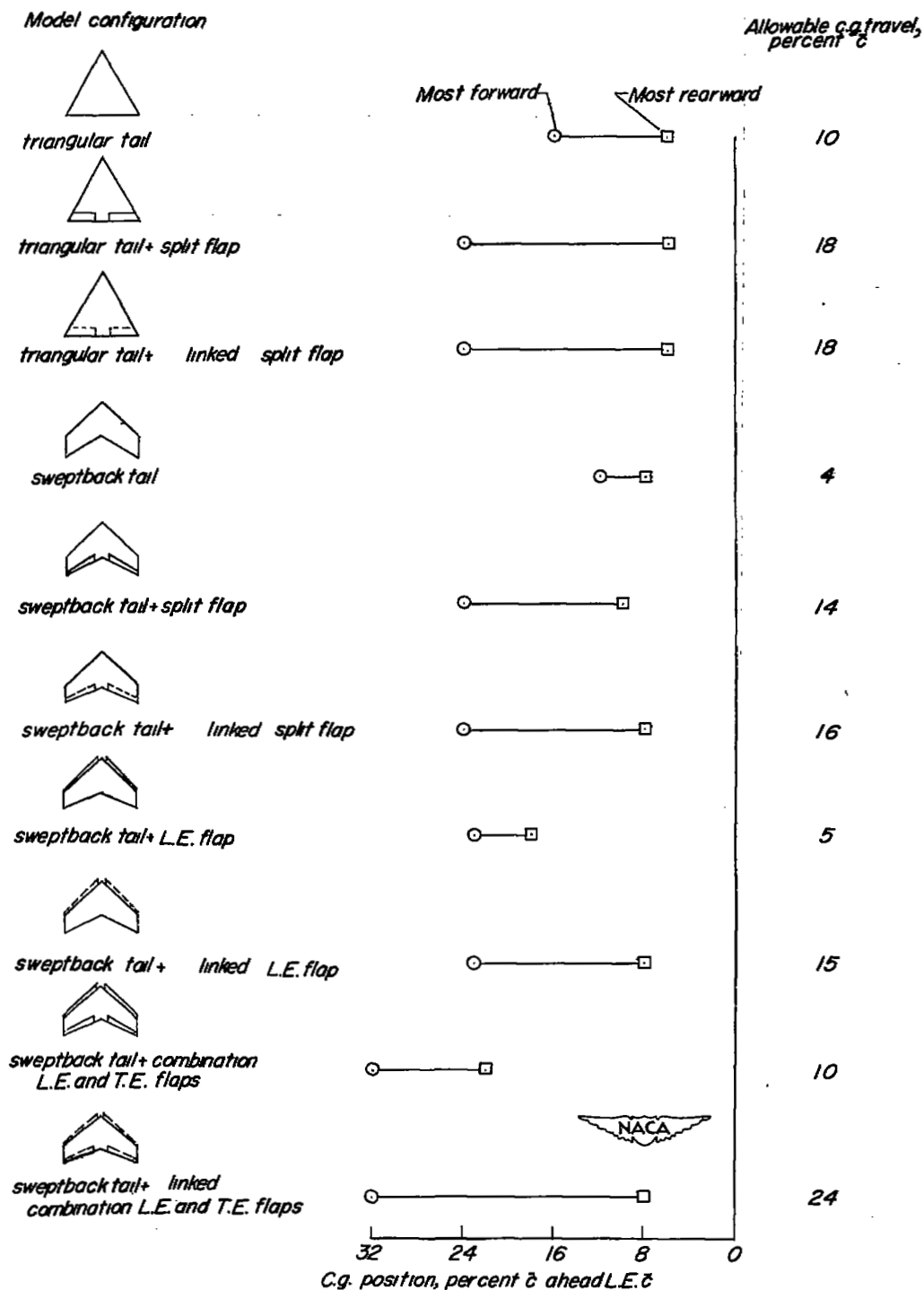
C.g. position, percent c̄ ahead L.E.c̄

Figure 8.- Summary plot of the allowable center-of-gravity travel for
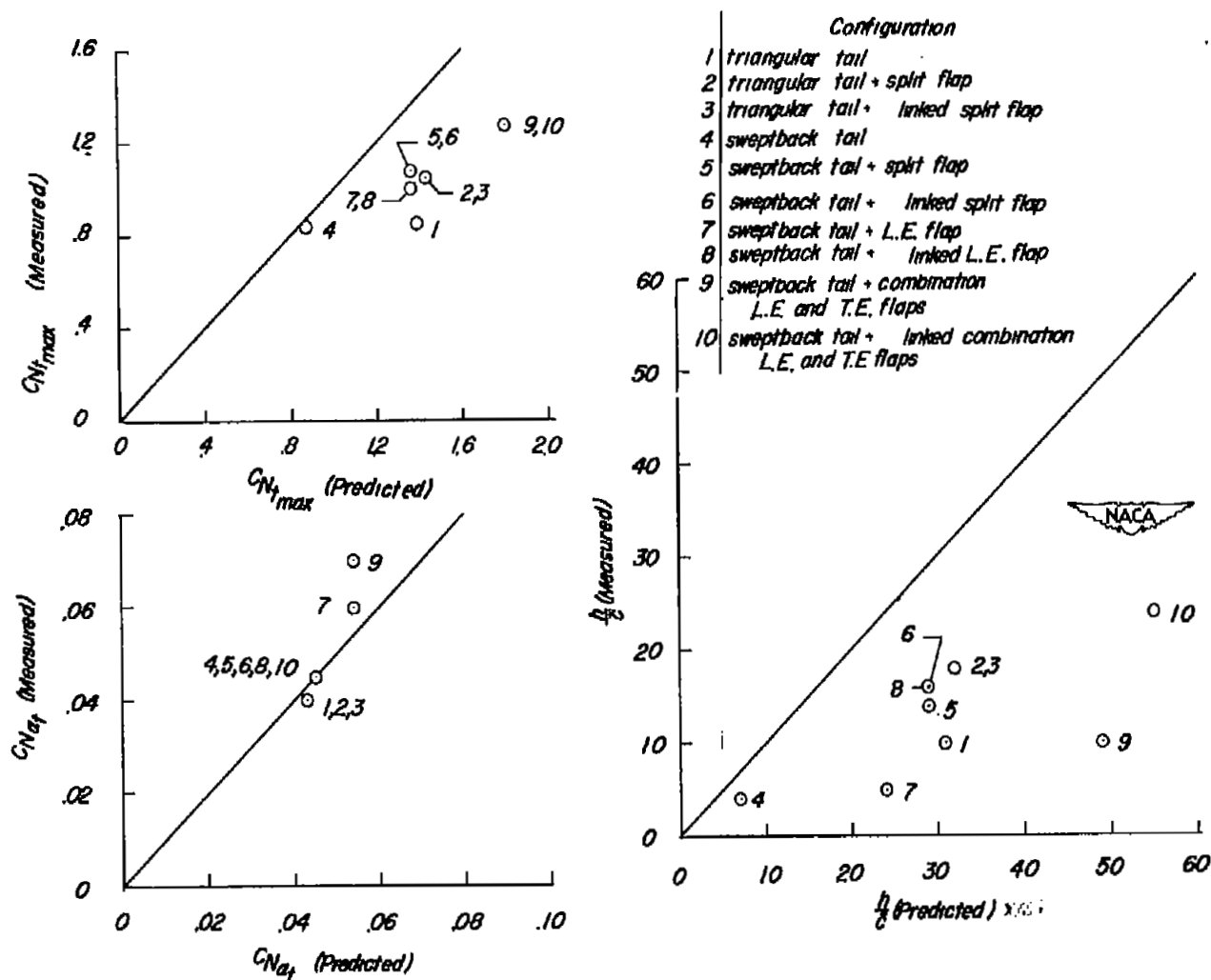the canard model with the various horizontal-tail configurations.

Figure 9.- Comparison of predicted and measured normal-force coefficients, slopes of the normal-force-coefficient curves, and allowable center-of-gravity travels.